

## Characterization of a carburized surface layer on an austenitic stainless steel <sup>☆</sup>

K. Farrell <sup>\*</sup>, E.D. Specht, J. Pang, L.R. Walker, A. Rar <sup>1</sup>, J.R. Mayotte

*Oak Ridge National Laboratory P.O. Box 2008, Oak Ridge, TN 37831, USA*

### Abstract

Characterization tests were made of a commercial carburization treatment that has shown promise for hardening the surfaces of the austenitic stainless steel target vessel of the Spallation Neutron Source against cavitation erosion and pitting caused by the action of pulsed pressure waves in the liquid mercury target. The findings support most of the provider's promotional claims. The high surface hardness and the thickness of the hardened layer are validated, as are the hardness-depth profiles. The austenite lattice of the layer is enlarged and placed in a state of compressive stress and the surface is plastically distorted by the treatment. The corrosion resistance of the surface in selected acid media is greater than that for untreated austenite. The treated surface is not brittle and is quite resistant to cracking during straining. The maximum carbon content of the layer is measured at 3–4.5 wt%, versus 6–7 wt% cited by the provider. Contrary to the provider's assertion that all of the carbon is contained in supersaturated solid solution in the austenite phase, some of the carbon is present in an iron carbide phase located non-uniformly at the very surface. Inclusion stringers and  $\delta$ -ferrite phase in the carburized layer are more prone to corrosion and may provide preferential sites for cavitation pitting.

Published by Elsevier B.V.

*Keywords:* Pitting; Carburization; Hardness; Lattice parameter; Surface analyses

### 1. Introduction

The vessel that holds the liquid mercury target in the Spallation Neutron Source (SNS) will be subjected to

pitting erosion due to collapse of cavities created in the mercury by the action of the pulsed proton beam. Techniques to mitigate the damage are under investigation. Generally, vessel materials with hard and tough surfaces are more resistant than softer ones. The material selected for construction of the SNS target vessel is 316LN grade austenitic stainless steel. It is not a hard material so various surface hardening techniques are being investigated to improve its cavitation pitting resistance. One technique that has shown good promise is a surface hardening treatment known as Kolsterising<sup>®</sup>. Kolsterising<sup>®</sup> is the registered trade name of a proprietary surface carburization treatment for austenitic alloys provided by Bodycote Metal Technology Group from

<sup>☆</sup> Research supported by the Spallation Neutron Source Project, managed by UT-Battelle, LLC, under contract DE-00OR22725 for the U.S. Department of Energy.

<sup>\*</sup> Corresponding author. Tel.: +1 865 574 5059/482 2354; fax: +1 865 574 0641.

*E-mail addresses:* [farrellk@ornl.gov](mailto:farrellk@ornl.gov), [kfspf@icx.net](mailto:kfspf@icx.net) (K. Farrell).

<sup>1</sup> ORNL and University of Tennessee, with support through the ShaRE program.

their division at Apeldoorn in The Netherlands, now available in the USA at Bodycote Kolsterising® North America, Boaz, Alabama. Special advantages are said to be high hardness and toughness; good resistance to pitting corrosion, stress corrosion, and crevice corrosion; increased resistance to wear and galling; and better fatigue properties.

According to Bodycote's promotional information [1], Kolsterising® is a process in which carbon is diffused into the surface of an austenitic alloy at low temperature. Details of the actual carburization treatment are proprietary. The amount of carbon introduced is 6–7 wt% at the surface, declining to zero at a depth that depends on the length of the treatment. Bodycote's regular 33 µm treatment purportedly affects a layer about 33 µm deep. Within the layer the infiltrated carbon is incorporated in supersaturated interstitial solid solution in the austenite phase. Accommodation of the carbon in the layer is claimed to cause expansion of the affected austenite crystal lattice that is opposed by the unexpanded, and unhardened, substrate. This imposes compressive stresses in the layer. These stresses, combined with the changes in chemical composition, significantly harden the material to a depth of about 33 µm. Hardness values of 1000–1200 DPN units (Vickers diamond pyramid number) are produced at the very surface and decline with depth to the substrate hardness of about 200 DPN at 30–40 µm.

SNS target vessels will be built to exacting standards and will be required to meet or exceed critical performance measures. If a Kolsterising® treatment is to be incorporated in the fabrication procedure, it is essential that the provider's claims be verified independently. To investigate Bodycote's claims and to uncover any factors that might be of concern for the integrity of a Kolsterised target vessel, some characterization tests of the nature of the surface layers of Kolsterised austenitic 316LN stainless steel have been conducted at ORNL. The results are described herein.

## 2. Characterization procedures

The characterization tests included optical metallographic examination, hardness tests, X-ray analyses for phase recognition and local stress determination, and electron microprobe chemical analyses. Two 10 mm diam. × 1 mm thick disk specimens, #C14 and #H4, were studied. Disk #C14, was one of a number of such disks prepared from 316LN stainless steel, Jessop heat #18474, for a series of cavitation pitting tests being conducted at the LANSCE facility at Los Alamos National Laboratory. This is the heat from which the first target vessel will be fabricated. Before Kolsterising®, disk C14 was machined and ground from plate stock, was vacuum annealed at 1050 °C, and one of its flat faces

was mechanically polished with 0.25 µm diamond paste. Disk #H4 was cut from a multi-pass TIG weld made to join two 2.0 mm thick annealed plates of a European-made 316 steel labeled EC316LN. Before Kolsterising, disk H4 was ground to 1.0 mm thick and one of its flat faces was polished with 0.25 µm diamond paste. Both disks were given the 33 µm Kolsterising® treatment by Bodycote.

## 3. Results for Kolsterised annealed disk C14

### 3.1. Surface distortion

Before Kolsterising®, the as-polished, exterior flat surface of the disk was mirror smooth and no microstructural features could be discerned except for some inclusions. After the Kolsterising® treatment, the surface was heavily wrinkled, grain boundaries were strongly demarked, and the grains contained extensive, coarse parallel slip and/or mechanical twin lines indicating the occurrence of considerable plastic deformation during Kolsterising®, Fig. 1. These features are surface relief markings visible without the aid of any metallographic etching. According to Bodycote, plastic deformation of the surface does occur during Kolsterising®. Closer examination of the deformed surface revealed the presence of a thin, discontinuous, spiny-like structure, almost hidden by the deformation bands. This structure was detected in all grains but was prominent in only few of them, as in the several lighter toned grains seen at higher magnification in Fig. 2. The structure is distinguished by the facts that its spines are shorter than the width of the grain and they lie in at least four orientations. In contrast, the deformation bands are linear and narrow, they usually span the full width of the grain, and they lie in only one or two directions except

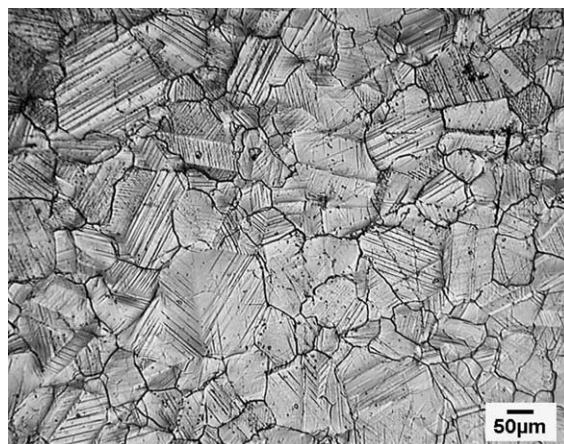


Fig. 1. Distorted surface after Kolsterising®.

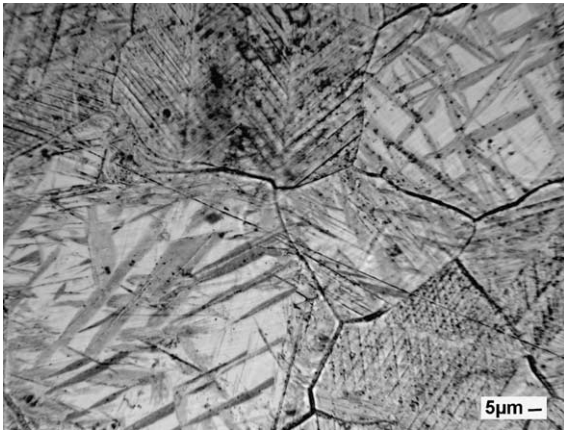


Fig. 2. Spiny structure in the deformed surface.

where they are perturbed by the presence of annealing twins. The reclusive, spiny feature is considered in more detail in Section 3.8.

### 3.2. Hardness

The hardness of the Kolsterised layer was measured in two ways, one directly on the flat surface and the other on a cross-section piece cut normal to the flat surface. The on-face tests were made to search for areal variation of hardness and to determine the effects of indentation load. Because the Kolsterised layer is quite thin, indentations made at normal microhardness loads of 500 g or so will penetrate through the layer and will sample both the layer and the unhardened substrate together, giving a falsely low measure of the layer hardness. Very light loads will test mostly the layer but the size of the indentation will be small and will be subject to appreciably larger errors of measurement. To optimize the surface hardness value Bodycote uses a load of 50 g. For such a load, Bodycote quotes Vickers pyramid hardness numbers (DPN) of 1000–1200 for Kolsterised austenitic stainless steel, which is a considerable increase over the normal value of about 200 DPN for untreated annealed austenitic stainless steel. No areal variations of hardness are quoted.

For our areal tests three regions on the originally polished face were chosen at random, and in each region seven tests were made at different loads between 50 and 2000 g. The results are shown in Fig. 3. They indicate good reproducibility from one region to another, implying no areal variation. They also show, very clearly, that with increasing load the contribution of the hardened layer to the composite hardness is reduced as more and more of the softer substrate is sampled. The average hardness measured at 50 g load is 1040 DPN, in agreement with Bodycote's hardness of 1000–1200 DPN for Kolsterised 316 stainless steel. The average hardness at

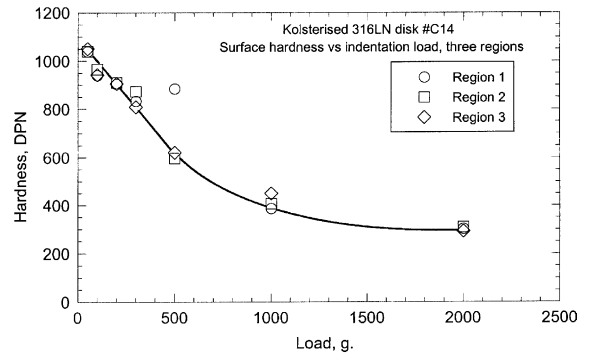


Fig. 3. Surface hardness as a function of indentation load at three randomly chosen regions on Kolsterised disk C14.

2000 g load is 301 DPN versus 259 DPN measured for the untreated material, indicating only modest influence of the presence of the layer at high loads.

Although these surface hardness tests showed no variation with areal location, it is cautioned that they represent only a small area. Later, we will show thickness variations in the Kolsterised layer. A reduced thickness might not affect the 50 g surface hardness nor the initial pitting resistance but it would impair the pitting resistance over time as the surface layer is eroded, and would shorten the service lifetime of the vessel.

Since the layer is created by inward diffusion of carbon, the concentration of carbon in the layer will decrease with depth, and likewise the hardness, which is supposedly governed by the concentration of carbon, will decrease with depth within the layer itself. To map such variation, hardness measurements must be made on a cross-section through the layer. Examples of cross-sectional hardness-depth profiles published by Bodycote for two Kolsterising® treatments, 22 and 33 μm in 316 stainless steel, are reproduced in Fig. 4.

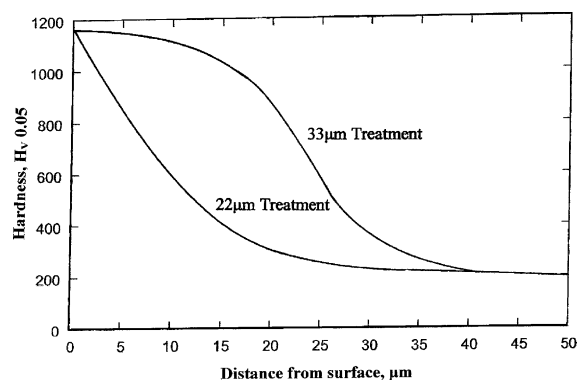


Fig. 4. Bodycote's hardness-depth profiles for 316 stainless steel.

For our determination of the hardness profile through the thickness of the layer, a chordal slice was cut from the disk and was mounted in cold-setting epoxy with the cut edge facing up. The edge of the slice was then polished to a mirror finish and was given a light etch. Using a load of 50 g, hardness traverses were made across the hardened layer into the substrate. To avoid the impressions influencing one another they were made along lines intercepting the Kolsterised surface at small angles and were spaced at intervals greater than three times the size of the impressions. On completion of a traverse, the perpendicular distances of the impressions from the surface were measured. The combined results from two traverses are displayed in Fig. 5. The data do not fully reproduce the shape of Bodycote's 33  $\mu\text{m}$  curve in Fig. 4.

Much of the lack of full correspondence between Figs. 4 and 5 is due to a distance limitation from the edge of the specimen at which reliable microhardness measurements can be made with a diamond pyramid indenter. That distance is set by the size of the hardness impression. The impression must not contact, or very closely approach, the edge of the piece or the edge will barrel outwards. The lack of support during barreling will give larger indentations and erroneously low hardness values. Indentations that were obviously barreled were ignored. However, the barreling is often not easy to discern because of the small size of the indentation and because the Kolsterised surface is not microscopically flat. The hardness of 1040 DPN given for zero distance in Fig. 5 is the surface hardness measured in Fig. 3 for a 50 g load, for which the impression had a diagonal width of 9.5  $\mu\text{m}$ . Since the region deformed by the indenter is usually about twice the width of the indentation any impression made on a cross-section piece at 50 g load within about 10  $\mu\text{m}$  of the edge of the piece will be subject to barreling. This is seen in Fig. 5 for the bunched data points around 700 DPN at distances of 8–15  $\mu\text{m}$ . Presumably, the hardnesses at distances less than 8  $\mu\text{m}$  are actually greater than 700 DPN. Bodycote's 33  $\mu\text{m}$  hardness profile in Fig. 3, which shows

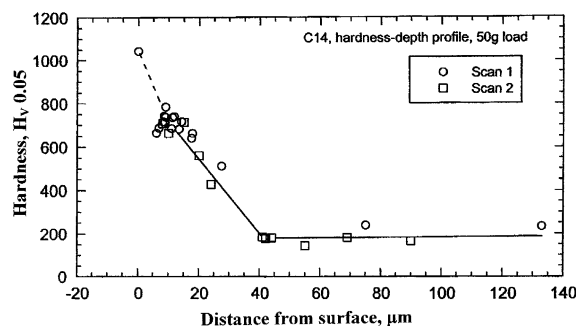


Fig. 5. Hardness-depth profile for Kolsterised disk C14.

hardness values >1000 DPN in this depth range must have been determined with a different technique, perhaps using a Knoop type indenter that allows a closer working distance to the edge. At greater distances beyond 15  $\mu\text{m}$ , where the measurements are more reliable, the hardness in Fig. 5 decreases to the parent metal value at a depth of about 40  $\mu\text{m}$ , in fair agreement with Bodycote's 33  $\mu\text{m}$  profile.

### 3.3. Toughness

Toughness was ascertained not from specific toughness tests but from other observations. During the surface hardness tests on the Kolsterised specimen, the hardness impressions were scrutinized for signs of brittleness in the layer. A brittle layer would crack under the deformation induced by penetration of the indenter, and the extent of the cracking should increase with the severity of the penetration. The scrutiny revealed that the indentations were surrounded by lightly dished regions containing fresh slip lines from plastic deformation of the layer occurring during the hardness test. Cracks were found in only 2 out of 59 impressions and were made under large loads of 1000 and 2000 g, which are considered to be extreme tests of the integrity of the layer. The cracks were located at the rim of the impression and just inside it, where tensile forces would be greatest. They were small, irregular, and discontinuous, not indicative of a brittle material. The conclusion was that the Kolsterised layer is plastically deformable and is tough, not brittle. This conclusion was bolstered by observations made during sawing and grinding of other Kolsterised specimens. When the tool was impinged on the Kolsterised layer from the direction of the mid-thickness of the specimen it forced the freshly cut, unsupported edge of the layer to rotate away from the tool through angles greater than 90°, creating free-standing curlicues of Kolsterised material with no cracks in them. This combination of high ductility and high hardness is unequivocal testimony of good toughness.

### 3.4. Corrosion resistance

No standard corrosion tests were conducted but during etching tests for metallographic preparation of the cross-section specimen it was apparent that the Kolsterised layer was much more resistant than the base 316LN alloy to corrosion attack by aqueous solutions containing various mixes of HCl, HNO<sub>3</sub>, and HF, and Glyceresia (30 parts each glycerol and HCl and 10 parts HNO<sub>3</sub>). These etchants all exposed the grain structure in the polished substrate steel but not in the polished Kolsterised layer. The unetched layer contrasted sharply with the etched substrate and could be seen with the naked eye as a thin white envelope wrapping the specimen, shown in Fig. 6 at low magnification. This resistance to etching



Fig. 6. Etched cross-section through Kolsterised disk C14.

agrees with Bodycote's claim of improved corrosion resistance.

### 3.5. Penetration front

Under visual inspection at low magnification, the penetration front of the Kolsterised layer seemed to be abrupt, Fig. 6. At higher magnification the apparently sharp demarcation line between the layer and the substrate is seen to be an optical deception; there is no line, the unetched layer simply merges with the etched substrate (see Figs. 7 and 8). There are no signs of a gradation or of preferential incursion along grain boundaries. This absence of a distinct physical interface boundary between the hardened surface and the relatively soft parent metal is indicative of atomic cohesion of the penetration front with the parent metal, and confirms that the hardened surface layer is not a separate layer or coat. It is an integral part of the steel. It is consistent with a diffusion-controlled, carbon penetration process, as asserted by Bodycote. The flatness of the front was relatively independent of the original surface roughness. It was equally flat on the previously mirror-like polished surface (lower edge in Fig. 6) as on the as-ground upper surface. However, at the short edges of the piece that were rough machined before Kolsterising<sup>®</sup>, the front was a little more irregular than at the ground and polished surfaces, and the outer surface of the layer was decidedly rougher.

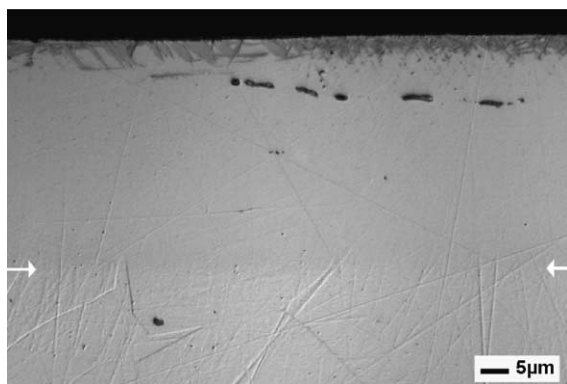


Fig. 7. Surface structure and etched-out inclusion stringer in the Kolsterised layer in disk C14.

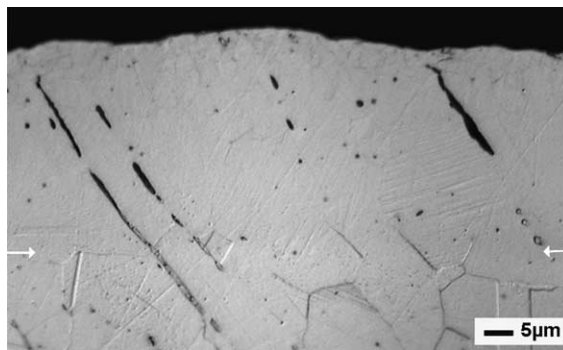


Fig. 8. Change in etching susceptibility of inclusion stringers crossing the Kolsterised front in 316L steel.

### 3.6. Variation in layer thickness

Uniformity of thickness of the Kolsterised layer on a target vessel will be a prerequisite for establishing a reliable performance lifetime for the vessel. Therefore, the thickness of the layer on the cross-section chordal piece used for the hardness-depth profiles was measured carefully. The layer was not uniformly thick, nor was the outer surface uniformly flat. The layer on the prepolished surface was dished near the center length of the piece. This tapered thickness is seen in the bottom surface in Fig. 6. There, the depth varied from a maximum of 42  $\mu\text{m}$  to a minimum of 12.5  $\mu\text{m}$  at the base of the dished layer. The depth of the layer was measured at other positions around the piece. On the as-ground surface the depth was a uniform  $38 \pm 2 \mu\text{m}$ . On the short, as-machined edges, the layer thickness varied between 55 and 77  $\mu\text{m}$ . The outer surface roughness was fairly smooth on the as-ground and prepolished surfaces but was much rougher on the as-machined edge surfaces. Kolsterising<sup>®</sup> treatments are normally conducted on specimens piled randomly in wire mesh baskets. So it is quite possible that the thin, dished region in the layer on the prepolished surface could be due to shielding by contact with a neighboring piece during Kolsterising<sup>®</sup>. No explanation is offered for the increased thickness and roughness at the edges of the piece. These thickness data are summarized in Table 1.

Table 1  
Summary of thickness measurements of Kolsterised layer

Location and prior surface condition	Layer thickness ( $\mu\text{m}$ )
Flat surface, polished, general	38–42
Flat surface, polished, one place	12.5
Machined edges	55–75
Weld, polished	37
Weld, parent metal, polished	40

### 3.7. Inclusions

Inclusions of unwanted residues from the steelmaking process can be expected even in the best steels. Inclusions have different chemical compositions than the austenite and they may respond differently to the Kolsterising<sup>®</sup> treatment. Their electrochemical potentials will not be the same as that for carburized austenite, and they may furnish preferred sites for pitting and corrosion. Such propensity could be greatly exaggerated in sheet and bar stock where forming operations have elongated the inclusions into stringers whose lengths might easily exceed the 30–40  $\mu\text{m}$  thickness of a Kolsterised layer. Any such stringers passing through the layer might be latent paths for cavitation pitting.

Disk C14 was remarkably low in inclusions and only one or two of the stringers intercepted the Kolsterised layer, none passing through it. An example of a stringer completely within the layer and lying at a small angle to the surface is shown in Fig. 7. The position of the penetration front of the layer is indicated by the arrows. The stringer is heavily etched compared with stringers in the substrate. A piece of a different steel, a 316L grade that contained many inclusion stringers, was also examined and it revealed numerous instances of stringers traversing the Kolsterised layer, as shown in Fig. 8. In this case, the inferior corrosion resistance of the stringers in the Kolsterised layer is demonstrated by fact that those portions of the stringers within the non-Kolsterised substrate are lightly etched whereas the portions of the same stringers lying within the Kolsterised region are eaten away. Clearly, the Kolsterising<sup>®</sup> treatment had an adverse effect on the corrosion resistance of the inclusion stringer. This did not happen with all stringers, so presumably their susceptibility to corrosive attack was dependent on their structure and chemical composition.

### 3.8. A surface phase

The outer surface of the Kolsterised layer was different than the deeper parts of the layer. Whereas the bulk of the layer was featureless when viewed edge-on, etching revealed that the outer 5  $\mu\text{m}$  depth contained a discontinuous structure with a highly irregular, spiny-like front shown clearly at the surface in the upper part of Fig. 7. This shallow structure corresponds to the mixture of plastic deformation and the spiny phase noted in Section 3.1. Surface plastic deformation resulting from Kolsterising<sup>®</sup> treatment is acknowledged by Bodycote but the spiny phase has not been reported. Interestingly, it was not present in the 316L specimen, Fig. 8. At first, it was thought that the spiny phase might be martensite caused by the plastic deformation of the surface during Kolsterising<sup>®</sup>. It is known that straining, either elastic or plastic, of Fe–Ni–Cr austenite can cause the formation of martensite [2,3]. However, the propensity for

martensite formation declines markedly with temperature above room temperature, and is reduced by austenite stabilizing elements such as carbon. Since the Kolsterising<sup>®</sup> treatment is presumably conducted above room temperature to reduce treatment time and to maximize the penetration of carbon, it seems unlikely that martensite will form during Kolsterising<sup>®</sup>. Nevertheless, a phase similar to  $\alpha'$ -martensite has been reported in the surface layer of 316 austenitic steel carburized in a methane gas plasma at 400–600  $^{\circ}\text{C}$  [4], but was not detected in other work conducted under the same conditions by the same authors on 316 and 304 steels [5].

To identify the spiny phase, X-ray diffraction analyses were made on the outer face of the as-Kolsterised surface and on an annealed, non-Kolsterised, control specimen of the 316LN steel. The intensity peaks are shown in Fig. 9. Several features are obvious. First, Kolsterising<sup>®</sup> has introduced many more peaks. Second, the austenite peaks in the Kolsterised specimen are much broader and are shifted to lower angles than those in the annealed specimen. Analysis of the data indicated that the Kolsterised surface contained roughly equal parts of expanded austenite phase and a carbide phase. The diffraction pattern from the carbide phase coincided most closely with  $\text{Fe}_5\text{C}_2$  Hagg ( $\gamma$ ) carbide. However, the lattice parameter of the phase was closer to  $\text{Mn}_5\text{C}_2$ . Two small lines were not assignable to  $\text{Fe}_5\text{C}_2$ . One of these coincided with a line for  $\text{Cr}_7\text{C}_3$ , but no other supporting lines were found for  $\text{Cr}_7\text{C}_3$  and therefore it was assumed that the chromium carbide phase was not present. The boxes at the base of Fig. 9 display the locations and scales of standard lines for martensite and  $\text{Fe}_5\text{C}_2$ . All of the standard  $\text{Fe}_5\text{C}_2$  lines are found in the spectrum

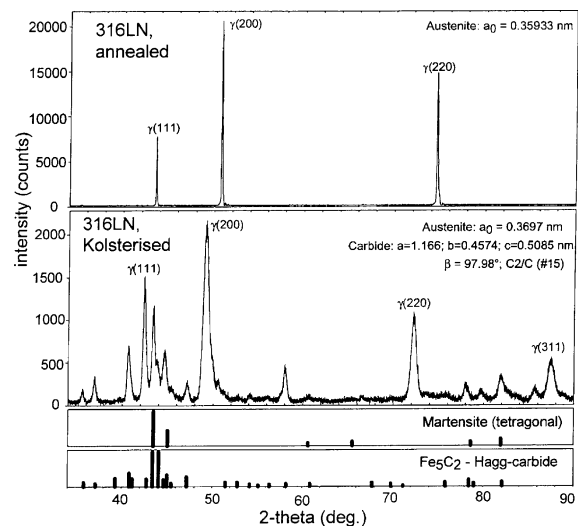


Fig. 9. X-ray diffraction peaks from 316LN steel before and after Kolsterising<sup>®</sup>.

from the Kolsterised specimen except for one at 39°. With regard to martensite phase, the search for it was thwarted by the fact that the positions of the martensite lines coincide with some of those for Fe<sub>5</sub>C<sub>2</sub>. Thus, the presence of martensite can not be verified nor rejected on this X-ray evidence. The carbide phase has many more lines than the martensite, and there is no question of its presence. According to the lattice parameter measurements, the carbide phase appeared to be free of stress.

### 3.9. Lattice expansion

The broadening and shifting of the primary reflections for the austenite phase in Fig. 9 are evidence of distortion and expansion of the austenite phase. Plastic distortion will widen the peaks, and expansion of the austenite lattice will displace the peak positions to smaller angles. Plastic distortion was undoubtedly present, as seen in Fig. 1. Large increases in lattice parameter,  $a$ , were measured. These increases will cause stresses and strains in the Kolsterised layer. At the surface, the austenite between the particles of the carbide-like phase had an in-plane lattice parameter,  $a_{in}$ , of 0.3681 nm and an out-of-plane value,  $a_{out}$ , of 0.3695 nm. The lattice strain is  $\varepsilon = (a_{in}/a_{out}) - 1$ , which gives a value of  $-0.0038$ . The lattice stress is  $\sigma = \varepsilon Y/(1 + \nu)$ . Using a Young's modulus,  $Y$ , of 193 GPa and a Poisson's ratio,  $\nu$ , of 0.3, the residual stress is estimated to be minus 550 MPa. This residual compressive stress is much larger than the normal yield strength of 205 MPa at room temperature and about 130 MPa at 300 °C for annealed 316LN steel [6], and it explains why the Kolsterising<sup>®</sup> process induces gross plastic deformation at the surface. Although plastic deformation widens the austenite peaks in Fig. 9 it should not change the lattice parameter of the austenite. The expanded lattice is presumed to be due to absorption of carbon in supersaturated solid solution. Published data [5] relating lattice parameter to dissolved carbon concentration for 316 stainless steel carburized with up to 2.5 wt%C at 450–500 °C shows a linear function,  $a = 0.3597 + 0.0054C$ , where  $C$  is wt% carbon. In the present work, the average  $a$  value measured for the expanded austenite at the surface is 0.3688 nm, which corresponds to a carbon concentration of 1.68 wt% in solid solution in the austenite. This is much smaller than the 6–7 wt%C claimed by Bodycote.

#### 3.9.1. Depth dependence of lattice expansion

The depth dependence of the expanded lattice parameter of the austenite in the Kolsterised layer was explored by analysis of the energies of the reflected beams using a small X-ray beam spot in the Advanced Photon Source at Argonne National Laboratory. To eliminate grain-to-grain variation the measurements were made on a single large grain that intercepted the

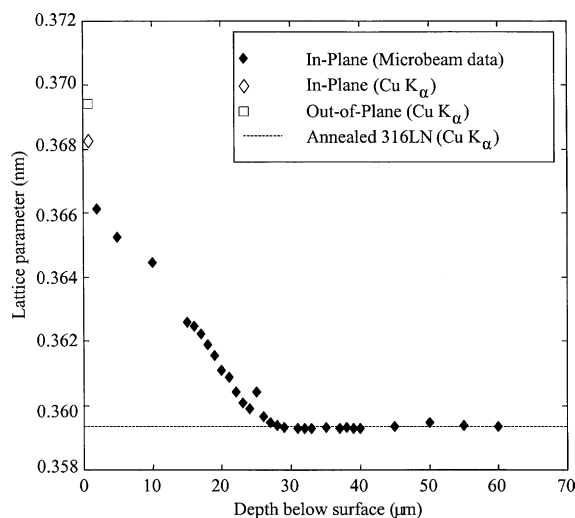


Fig. 10. Variation of the austenite lattice parameter with depth.

surface. The results are presented in Fig. 10. They show that the expansion of the austenite lattice parameter is a maximum at the surface and progressively decreases with depth into the layer, reaching the value for annealed, non-Kolsterised steel at a depth of about 30 μm. The shape of this profile is similar to the hardness-depth profile in Fig. 5.

### 3.10. Chemical analyses depth profiles

Chemical compositions as a function of depth were determined using an electron beam probe. This technique bombards the surface of the specimen with electrons and analyses the characteristic X-rays emitted by the surface atoms. Depth analyses were made on the polished cross-section through the Kolsterised layer. Three depth scans were made at randomly selected locations. Composition profiles found for the major metallic alloying elements of the steel are given in Fig. 11. It is evident that the relative concentrations of the original alloy elements in the steel did not change over most of the depth in the Kolsterised layer. However, at shallow depths of 0–2 μm or so, all the elements show small reductions in concentrations of a few percent. These reductions are mostly recovered at depths of about 5 μm, followed by asymptotic recovery to the base alloy compositions at depths of about 10 μm. This recovery pattern is most obvious in the Fe data which has the highest concentration values. These small decreases in major alloy elements at shallow depths can be accounted for by the carbon concentration profiles presented in Fig. 12. The carbon concentration of the base 316LN steel before Kolsterising<sup>®</sup> is 0.030 wt%. The measured carbon depth profiles are confounded by carbon contamination at about 0.5 wt% level from oils in the probe's vacuum

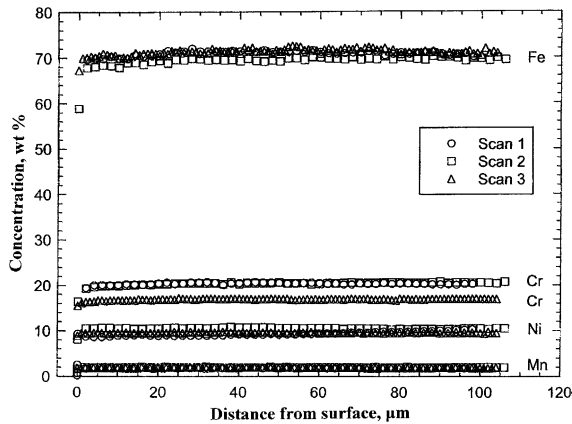


Fig. 11. Electron microprobe analyses of major metallic elements through the thickness of the Kolsterised layer at three locations.

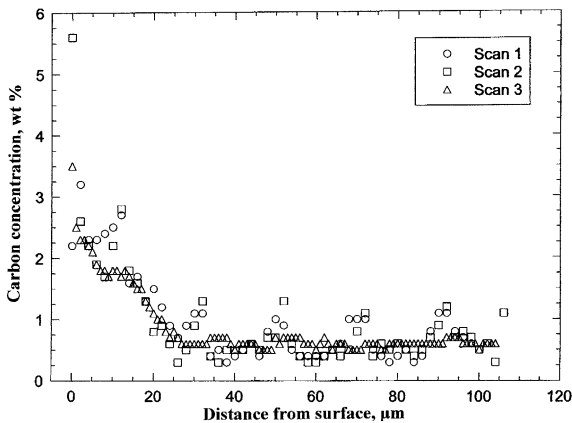


Fig. 12. Electron microprobe analyses of carbon through the thickness of the Kolsterised layer at three locations.

system, and by inexplicable ripples in the data. The ripples are smallest in scan 3 where it is clear that the carbon concentration is largest at the very surface and decreases with depth to the base value at 25–30  $\mu\text{m}$ . The maximum carbon level at the Kolsterised surface, less the contamination background, is about 5 wt% for scan 2, which has the largest decreases in the major metallic alloying elements, and is 2.5–3 wt% for scans 1 and 2. The overall shapes of the carbon profiles with depth are similar to those for the hardness-depth profiles and the austenite lattice parameter-depth profile. The large variation in carbon concentration for the scans in the near-surface regions can be attributed to random sampling of the mixture of expanded austenite and the discontinuously distributed  $\text{Fe}_5\text{C}_2$  phase by the electron beam. The austenite phase at the surface contains about 1.7% C according to Section 3.9. The carbide phase,

which showed no lattice expansion, should have a stoichiometric carbon concentration of about 7.9 wt%. The sample volume from which X-rays are emitted under the electron beam is a cubic micrometer or more, which would undoubtedly encompass fractions of the carbide phase. Thus some of the 2.5–5 wt% C found at the surface is presumably derived from the  $\text{Fe}_5\text{C}_2$  located in the outer surface region.

Limited attempts were made to examine the microstructures in the Kolsterised region by transmission electron microscopy (TEM) but were unsuccessful because the foils thinned preferentially at the deformation bands, and the regions between the bands were too thick for other features to be discerned.

#### 4. Results for Kolsterised TIG weld H4

##### 4.1. Surface distortion of the weld

The surface of the TIG (tungsten inert gas) weld, which was ground and polished to a 0.25  $\mu\text{m}$  finish before Kolsterising<sup>®</sup>, became distorted during Kolsterising<sup>®</sup>. The degree of distortion in the weld seemed to be no worse than that in the unwelded parent metal.

##### 4.2. Cross-section of the weld

A portion of the Kolsterised weld was examined in a polished-and-etched cross-section. The thickness of the Kolsterised layer on the weld was uniform at about 37  $\mu\text{m}$ , versus about 40  $\mu\text{m}$  for the layer on the parent metal. Large thickness variations like those seen in the unwelded C14 disk were not found. The microstructure of the weld was quite different from the bland equiaxed austenite grains of the base metal. The weld grains were lamellar and contained thin, elongated zones of a discontinuous phase. The morphology of the phase, shown in Fig. 13, is characteristic of the delta ( $\delta$ ) ferrite phase usually found in fusion welds in austenitic steels [7,8], and was not altered by the Kolsterising<sup>®</sup> treatment. However, the particles of ( $\delta$ ) ferrite phase embraced by the Kolsterised layer were etched away more readily than the normal ( $\delta$ ) ferrite phase lying below the layer. This observation agrees with Bodycote's advice that, compared to austenite,  $\delta$ -ferrite will not respond well to Kolsterising<sup>®</sup>, and duplex structures of austenite and  $\delta$ -ferrite may not deliver uniformity of properties in the Kolsterised layer.

##### 4.3. Hardness of the weld

Results of hardness-depth profiles measured on the cross-section piece of H4 across the thickness of the Kolsterised layer and into the substrate, one at the weld and the other on the base metal, are shown in Fig. 14. The

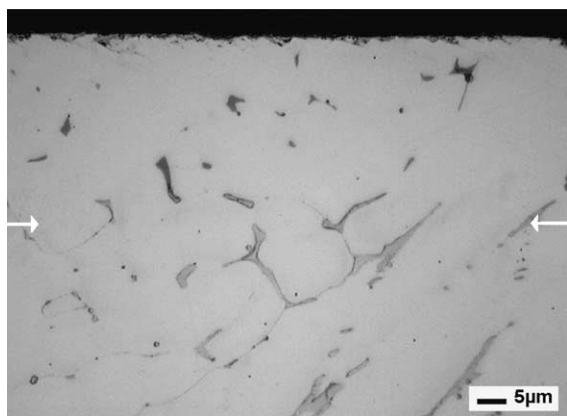


Fig. 13. Etched Kolsterised layer in weld structure.

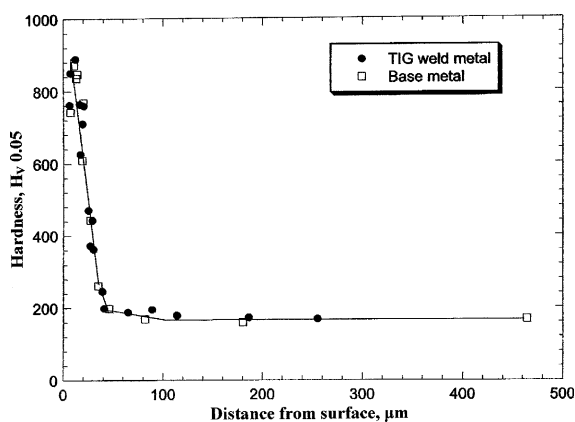


Fig. 14. Through-depth hardness profiles in Kolsterised weld specimen H4.

two sets of data follow a single profile, compatible with the data described earlier for specimen C14. One conclusion from this data is that the Kolsterised layer on the weld is no softer than that on the base metal. Another conclusion is that the presence of the  $\delta$ -ferrite phase does not degrade the hardness of the 316LN steel weld, both inside and outside the Kolsterised layer. It is reported [7] that despite differences in crystal structure and chemical composition the hardness of  $\delta$ -ferrite in welds in non-Kolsterised austenitic stainless steel is comparable with the hardness of the austenite. Also, the  $\delta$ -ferrite phase in the weld is thermally unstable at temperatures above about 475 °C [7,8] and undergoes decomposition to G phase and  $M_{23}C_6$  carbide, with attendant increase in hardness [7,8]. Therefore, the heat pulses suffered in multi-pass welds could cause the hardness of the  $\delta$ -ferrite to vary. It is not publicly known what a Kolsterising<sup>®</sup> treatment will do to the  $\delta$ -ferrite phase, but Bodycote recommends that materials offered for Kolsterising<sup>®</sup> treatment should be ferrite-free. For the hard-

Table 2

Nanohardness values in the austenite matrix and in the  $\delta$ -ferrite phase in the Kolsterised weld metal

Test #	$\delta$ -ferrite, GPa	Test #	Austenite, GPa
1	6.0	6	7.4
2	2.8	7	8.4
3	10.7	8	8.1
4	5.9	9	8.7
5	12.3	10	8.3

ness measurements in Fig. 14, it should be recognized that the packets of  $\delta$ -ferrite phase are narrow, 2  $\mu$ m or less, compared to the width of a microhardness indentation in the layer, which is of order 10  $\mu$ m. Thus, the hardness indentations encompass a much larger volume of austenite than  $\delta$ -ferrite and the hardness value will not be strongly sensitive to participation by the  $\delta$ -ferrite. In view of Bodycote's cautionary advice on  $\delta$ -ferrite an attempt was made to ascertain whether the hardness of the  $\delta$ -ferrite phase in the Kolsterised layer in the weld layer was different than its surrounding austenite. The features and the surrounding matrix were probed with a nanohardness tester. The results are given in Table 2. These nanohardness data values should not be compared directly with the earlier microhardness data; some scaling calibration is required.

It can be seen in the table that five measurements made on the austenite matrix gave fairly reproducible nanohardness values of 7–8 GPa. Five measurements attempted on five of the  $\delta$ -ferrite areas were not so consistent, giving values that ranged from about 3 to 12 GPa. In one of these latter cases, the 6.0 GPa value, it was found that the indentation missed the  $\delta$ -ferrite particle. Some of the particles were partially etched out. It was concluded that this short exercise to test the relative hardnesses of the  $\delta$ -ferrite and the austenite phases in the Kolsterised portion of the weld indicated significant hardness variation in the  $\delta$ -ferrite but would require considerably more effort to give meaningful data.

## 5. Discussion and conclusions

The results of these characterization tests verify most of the promotional claims made by Bodycote for its Kolsterising<sup>®</sup> treatment. The surface hardness claims are substantiated, as are the hardness-depth profiles. The surface is distorted by the treatment, and the austenite lattice is enlarged, as stated by Bodycote. The lattice expansion-depth profile and the carbon-depth profiles are similar to the hardness-depth profile. The corrosion resistance of the Kolsterised layer in certain acid media is greater than that for untreated austenite. The layer is not brittle; it is plastically deformable and is quite resistant to cracking during straining. Contrary to

Bodycote's assertions, the maximum carbon content of the layer is much less than 6–7 wt%, and the carbon is not simply contained in supersaturated solid solution; much of it seems to be present in a previously unreported iron carbide phase located non-uniformly at the very surface. Inclusions and  $\delta$ -ferrite phase that were encompassed by the Kolsterised layer became more sensitive to acid etching. Generally, many of these observations are similar to those described elsewhere [4,5] for a plasma carburizing process conducted at temperatures between 300 and 600 °C.

The hardness and toughness of the Kolsterised layer are impressive. The surface hardness is about 1040 DPN, which is more than five times the hardness of the annealed 316LN steel. The mechanism of the hardening is not fully clear. Bodycote's literature cites a surface hardness of 1000–1200 DPN and implies that it is due entirely to the presence of 6–7 wt% C entrained in supersaturated solid solution in the austenite. The carbon concentration profiles, austenite lattice parameter measurements and associated estimate of expansion stress determined herein agree in principle that some of the hardening ensues from solid solution hardening, but disagrees with Bodycote on the quantitative aspects. If Bodycote is correct, and if the rate of solid solution hardening scales linearly with carbon concentration, each 1% C will raise the hardness by about 140 DPN above the substrate hardness of 200 DPN. Therefore, our measured maximum carbon concentration of 1.7% in solid solution deduced from the expanded lattice parameter, will yield a surface hardness of about 440 DPN, which is far short of the measured hardness of 1040 DPN. However, the plastic deformation associated with the Kolsterising<sup>®</sup> treatment will cause work hardening. Also, the carbide phase will undoubtedly be harder than austenite. It is suggested, therefore, that the balance of the increase in the hardness of the Kolsterised layer is provided by contributions from these two features.

Only the outer 10–15  $\mu\text{m}$  of the layer is at maximum hardness. Although this thin layer is strong and tough it is not an armor plate. It can be penetrated by a sharp edge, as testified by the surface hardness measurements made under different loads in Fig. 3. This implies that the Kolsterised layer will not be immune to mishandling damage by scratches and dents during installation of the target vessel in the SNS. A scratch visible to the naked eye might be 10  $\mu\text{m}$  deep and will create a softened trough in the layer. Such damage will not be repairable except by a repeat Kolsterising<sup>®</sup> treatment. If the layer is breached, the cavitation erosion rate at the breach will probably be the relatively high rate for the untreated substrate. Care will be needed to avoid such accidental damage.

The  $\text{Fe}_5\text{C}_2$  phase found in disk C14 but not seen in the Kolsterised 316L steel is not mentioned in Body-

cote's literature, nor was it encountered in other carburization treatments made at higher temperatures [4,5]. Whether this phase is specific to the LN grade steel or whether its formation is sporadic is not clear.

The thickness of the 33  $\mu\text{m}$  Kolsterised layer on disk C14 was quite variable. On disk H4 the layer was more uniform. A longer Kolsterising<sup>®</sup> treatment that gives a thicker layer of about 45  $\mu\text{m}$  is available but judging from the wide variation in thickness measured in specimen C14, +30%/-60% of the nominal 33  $\mu\text{m}$ , there is no guarantee that the extra thickness will be any more uniform or any more beneficial than the 33  $\mu\text{m}$  treatment. Specimen C14 was selected at random for this work, and the layer thickness variations found in it are disturbing. Although the resistance of the layer to cavitation pitting is promising, its performance over long periods will presumably vary with its thickness. Reliable prediction of vessel lifetime will depend, among other factors, on attainment of a uniformly thick Kolsterised layer on the most susceptible parts of the target vessel surface.

The observations that the Kolsterising<sup>®</sup> treatment seems to render some inclusions and the  $\delta$ -ferrite phase more susceptible to etching than the treated austenite implies reduced corrosion resistance for those microstructural features and thereby flags them as potential pitting corrosion sites. That does not necessarily make them the premier cavitation pitting sites. But if there is a connection between pitting corrosion susceptibility and cavitation pitting it becomes more significant because of the possibility the  $\delta$ -ferrite and inclusion stringers might provide short cut paths through the Kolsterised layer. The  $\delta$ -ferrite phase is networked through the layer. The inclusion stringers, depending on their orientation, can penetrate more directly through the layer, like tunnels. As such, they may offer preferred sites for pitting under the action of the pressure pulses during SNS service, possibly becoming deep 'drill holes'. Such drill holes have been observed in cavitation pitting simulation tests, and further tests of Kolsterised specimens in an ultrasonic vibration system are showing preliminary signs that inclusions are choice pitting locations [9]. If these locations become drill holes and allow leakage of mercury through the wall they will prematurely shorten the service lifetime of the target vessel irrespective of the general rate of erosion of the vessel.

Inclusions can be reduced by good steelmaking practice but it is unlikely they can be completely eliminated. Steps can be taken to minimize their effects on the SNS target vessel by paying attention to them during fabrication of the vessel, more specifically, by controlling their orientation with respect to the vessel wall thickness. When a cast steel billet is processed into bar or plate stock by forging, extrusion, or rolling, clusters of inclusions become strung out in the direction of the length of

the product. If these stringers are induced to lie parallel to the surface of the vessel wall they will be less likely to provide short-circuit drill hole paths through the wall than if they lie perpendicular to the wall. In that regard, a vessel fabricated from rolled sheet would be preferable to one machined from a large billet. In a formed sheet metal vessel the stringers will follow the curvature of the rounded nose of the vessel. In a vessel machined from a billet the stringers will pass through the wall at the curved nose, an undesirable situation.

With regard to the TIG weld, the hardness of the Kolsterised weld metal is the same as that of the Kolsterised base metal, despite seemingly large variations in the nanohardness of selected  $\delta$ -ferrite phase particles in the weld. If Kolsterising<sup>®</sup> confers pitting resistance to the austenite by virtue of raising its hardness, the presence of a small fraction of  $\delta$ -ferrite phase in a weld might not cause large variation in pitting resistance. Indeed, cavitation pitting tests made under ultrasonic vibration and reported in this Workshop Proceedings [9] show that Kolsterised welds in 316LN steel have similar erosion resistance to the Kolsterised base metal. If the  $\delta$ -ferrite phase does eventually become a pitting issue it can be handled easily by eliminating the  $\delta$ -ferrite phase or by placing the welds in the target vessel in positions where they will not be in contact with mercury. Elimination of  $\delta$ -ferrite phase can be achieved by using weld filler materials that stabilize austenitic phase and/or by post-weld heat treatments.

The target vessel design contains deep, narrow internal passageways that are required to be hardened like the external surfaces. Because the passageways have open entries, Bodycote expects that the layer produced on the inside surfaces of the deep passageways will be the same as that on more open surfaces and flat sections. To check that the layer thickness is independent of the particular geometry of the SNS target, a large section of the nose portion of a mock-up of a full size target has been Kolsterised and has been cut and examined to provide a map of layer thickness and hardness. The results are reported elsewhere in these proceedings [10].

Another concern with a Kolsterised layer is whether it will lose its hardness during the intense irradiation by protons and neutrons that a SNS target will experience. Atomic displacement and migration during irradiation might cause phase changes or may relieve internal stresses. In which cases, the hardness of the layer might fall. To investigate this prospect, an irradiation experiment with Kolsterised specimens is underway in the High Flux Isotope Reactor.

### Acknowledgements

We thank J.D. Hunn for providing specimen C14, and K.A. Yarborough and E.A. Kenik for attempting the TEM work.

### References

- [1] Kolsterising<sup>®</sup>, a hard copy of a CD ROM dated August 2001, distributed by Bodycote Metal Technology; and some hard-copy fliers. Also, communications with Bodycote personnel.
- [2] T. Angel, *J. Iron Steel Inst.* 177 (1954) 165.
- [3] Dieter Fahr, *Met. Trans.* 2 (1971) 1883.
- [4] Y. Sun, X. Li, T. Bell, *Surf. Eng.* 15 (1999) 49.
- [5] Y. Sun, X. Li, T. Bell, *Mater. Sci. Technol.* 15 (1999) 1171.
- [6] ASME Boiler and Pressure Vessel Code, Section II – Materials, Part D – Properties, 1998 Edition, July 1, 1998, The American Society of Mechanical Engineers, New York, New York.
- [7] S.A. David, J.M. Vitek, J.R. Keiser, W.C. Oliver, *Welding J.* (1987) 235.
- [8] J.M. Vitek, S.A. David, D.J. Alexander, J.R. Keiser, R.K. Nanstad, *Acta Metall. Mater.* 39-4 (1991) 503.
- [9] S.J. Pawel, Oak Ridge National Laboratory, private communication, 2003; S.J. Pawel, *J. Nucl. Mater.*, these Proceedings. doi:10.1016/j.jnucmat.2004.10.170.
- [10] D.C. Lousteau, T.J. McManamy, S.M. Chae, B.W. Reimer, K. Farrell, *J. Nucl. Mater.*, these Proceedings. doi:10.1016/j.jnucmat.2005.01.026.